Appl. Phys. A 87, 259–264 (2007)
DOI: 10.1007/s00339-006-3815-6

Applied Physics A
Materials Science & Processing

V. YANNOPAPAS[1,2]

Artificial magnetism and negative refractive index in three-dimensional metamaterials of spherical particles at near-infrared and visible frequencies

[1] Department of Physics, Sofia University, James Bourchier 5 Blvd., 1164 Sofia, Bulgaria
[2] Department of Materials Science, University of Patras, 26504 Patras, Greece

Received: 8 August 2006/Accepted: 15 November 2006
Published online: 25 January 2007 •

ABSTRACT In this paper, we present a new class of 3D metamaterials that exhibit artificial magnetism and/or negative refractive index. These metamaterials consist of spherical particles made from strongly resonant materials such as ionic/semiconductor materials and noble metals. Their electromagnetic response is studied using the extended Maxwell–Garnett effective medium theory and an ab initio method based on multiple scattering theory. The agreement between both treatments is very good, rendering the effective medium approximation a useful guide for the experimentalist in the field.

PACS 42.70.Qs; 42.25.Bs; 78.67.Pt; 78.67.Bf; 73.20.Mf

1 Introduction

One of the newest and most exciting research fields in classical optics is that of metamaterials. The latter are man-made structures that exhibit artificial magnetic response and/or negative refractive index (NRI) in certain frequency regions [1–3]. The magnetic response can lead to strong paramagnetic (permeability $\mu > 1$) and diamagnetic response (permeability $\mu < 1$ or even $\mu < 0$) of the same metamaterial structure in frequency regions where such a response is not met in naturally occurring materials, such as the near-infrared and optical regions. When the metamaterial structure also possesses negative permittivity ε in a frequency window that overlaps with the negative-μ region, an NRI n occurs. Most experimental realizations of magnetic metamaterials are based on metallic split-ring resonators (SRRs) and variations of such [4, 5]. The electric activity is achieved by use of thin metallic wires. When metallic SRRs and thin wires with the proper geometrical parameters are combined, an NRI occurs [6–8].

In this paper, we show that a strong magnetic response as well as NRI can be achieved by structures of simpler geometry than that of SRRs. Namely, 3D arrays consisting of spheres of an ionic or semiconductor material possess an effective (average) negative permeability μ_{eff} as a result of the giant values their dielectric function assumes around a certain frequency [9–14]. When such spheres are combined with metallic spheres possessing negative permittivity ε_{eff} in an overlapping frequency region so that a binary composite is formed, an NRI is evident [9]. To study these structures theoretically, the extended Maxwell–Garnett (EMG) effective-medium theory is used. The latter provides the required μ_{eff} and ε_{eff} of the above structures. The predictions of the EMG theory are in agreement with those of a rigorous, layer-multiple-scattering (LMS) method.

Following another route, a crystal with chiral symmetry consisting solely of metallic or ionic/semiconducting spheres can also exhibit NRI [15] based on a different mechanism [16, 17]. Their electromagnetic (EM) response is, again, studied by use of the LMS method. It is found, in particular, that such chiral structures exhibit NRI in several frequency windows rendering them as viable alternative to the mainstream NRI metamaterials.

This paper is organized as follows: in Sect. 2, the magnetic response of arrays of ionic/semiconducting spheres is theoretically studied. In Sect. 3, it is shown how one can achieve NRI by combining ionic/semiconductor spheres with metallic ones. In Sect. 4, the subject of chirality-induced NRI is discussed, and Sect. 5 concludes the paper.

2 Artificial magnetism from collections of polaritonic spheres

The basic methodological tool in our study is the EMG theory, which is briefly presented below. A composite material of spherical scatterers can be described, in the subwavelength limit, as a homogeneous medium of effective relative permittivity ε_{eff} and effective relative permeability μ_{eff}. We assume that the scatterers possess a relative permittivity ε_{s} and relative permeability μ_{s} and are embedded in a host medium described by a relative permittivity ε_{h} and relative permeability μ_{h}. The volume filling fraction occupied by the scatterers is denoted by f. ε_{eff} and μ_{eff} can be calculated from the extended Maxwell–Garnett theory (EMG) [18, 19], which goes one step ahead the ordinary Maxwell–Garnett theory by incorporating characteristics of Mie scattering in the corresponding formulae of ε_{eff} and μ_{eff}, i.e.,

$$\varepsilon_{\text{eff}} = \varepsilon_{\text{h}} \frac{x^3 - 3\mathrm{i} f T_1^E}{x^3 + \frac{3}{2}\mathrm{i} f T_1^E}\,, \tag{1}$$

✉ Fax: +30 2610 437394, E-mail: vyannop@upatras.gr

and

$$\mu_{\text{eff}} = \mu_{\text{h}} \frac{x^3 - 3\text{i}f\,T_1^H}{x^3 + \frac{3}{2}\text{i}f\,T_1^H}\,, \tag{2}$$

where T_1^E (T_1^H) are the electric-dipole (magnetic-dipole) components of the scattering T-matrix of a single sphere. They are given by

$$T_1^E(\omega) = \left[\frac{j_1(x_\text{s})\,[x j_1(x)]'\,\varepsilon_\text{s} - j_1(x)\,[x_\text{s} j_1(x_\text{s})]'\,\varepsilon_\text{h}}{h_1^+(x)\,[x_\text{s} j_1(x_\text{s})]'\,\varepsilon_\text{h} - j_1(x_\text{s})\left[x h_1^+(x)\right]'\,\varepsilon_\text{s}}\right],$$
$$T_1^H(\omega) = \left[\frac{j_1(x_\text{s})\,[x j_1(x)]'\,\mu_\text{s} - j_1(x)\,[x_\text{s} j_1(x_\text{s})]'\,\mu_\text{h}}{h_1^+(x)\,[x_\text{s} j_1(x_\text{s})]'\,\mu_\text{h} - j_1(x_\text{s})\left[x h_1^+(x)\right]'\,\mu_\text{s}}\right], \tag{3}$$

where j_1 (h_1^+) is the spherical Bessel (Hankel) function of order one and $[x j_1(x)]' = \mathrm{d}\,[z j_1(z)]\,/\,\mathrm{d}z|_{z=x}$ etc. x stands for the sphere size parameter, $x \equiv \sqrt{\varepsilon_\text{h}\mu_\text{h}}\omega S/c = 2\pi S/\lambda$, where S denotes the sphere radius and λ is the wavelength in the host medium. Also, $x_\text{s} \equiv \sqrt{\varepsilon_\text{s}\mu_\text{s}}\omega S/c = 2\pi S/\lambda_\text{s}$, where λ_s is the wavelength in the sphere medium. Equations (1) and (2) are valid in the quasi-static limit, i.e., provided that $x \ll 1$ but not necessarily $x_\text{s} \ll 1$, as it is the case for the ordinary Maxwell–Garnett formula (static limit) [18, 19].

A 3D array of nonoverlapping polaritonic spheres is considered. The electric permittivity of the spheres is given by [20]

$$\varepsilon(\omega) = \varepsilon_\infty \left(1 + \frac{\omega_\text{L}^2 - \omega_\text{T}^2}{\omega_\text{T}^2 - \omega^2 - \text{i}\omega\gamma_1}\right), \tag{4}$$

where ε_∞ is the asymptotic value of the dielectric permittivity at high frequencies, γ_1 is the loss factor, and the respective ω_T and ω_L are the transverse and longitudinal optical phonon frequencies. To begin with, losses are ignored in the polaritonic spheres by setting $\gamma_1 = 0$ in (4). As can be easily inferred from (1) and (2), the resonances of the T_1^H and T_1^E introduce resonances in μ_eff and ε_eff, respectively (although not at the same frequencies). Around these resonances, μ_eff and ε_eff may assume negative values, a fact which can be exploited for the realization of a metamaterial.

As a polaritonic material, the choice is $LiTaO_3$ whose permittivity is given by (4) having $\omega_\text{T} = 26.7 \times 10^{12}$ rad/s, $\omega_\text{L} = 46.9 \times 10^{12}$ rad/s, and $\varepsilon_\infty = 13.4$ [21]. The radius of the spheres is $S = 2.8\,\mu$m and the volume filling fraction occupied by them is $f = 0.736$. Of course, such a high value of f is possible only in fcc or hcp arrangements. In Fig. 1a the real and imaginary parts of μ_eff are shown, as calculated from (2) for the above collection of $LiTaO_3$ spheres. A region where the real part of μ_eff is negative is identified, namely from $\omega/\omega_\text{T} = 0.900$ to $\omega/\omega_\text{T} = 0.948$. This region corresponds to the first resonance of T_1^H.

As stated in the introduction, in order to ensure the validity of the EMG theory (1)–(3) against an ab initio method, one can consider a periodic realization of the $LiTaO_3$ particle array examined above. Namely, it is assumed that the $LiTaO_3$ spheres occupy the sites of an fcc lattice. For the sphere parameters considered above, i.e., $S = 2.8\,\mu$m and $f = 0.736$, the corresponding fcc lattice constant is $a = 7.94\,\mu$m. The

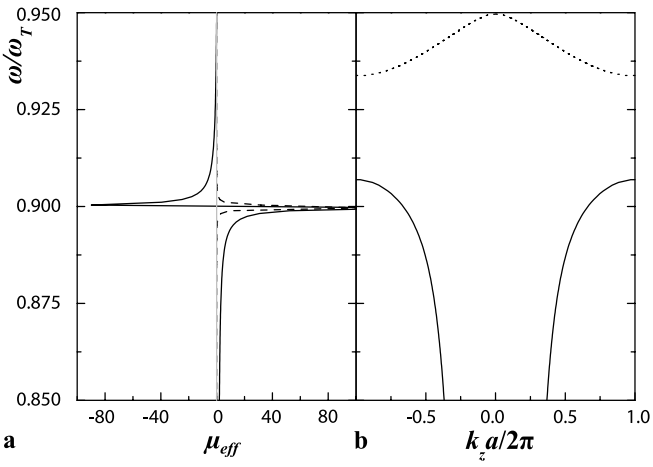

FIGURE 1 (**a**) The real (*solid line*) and imaginary (*broken line*) parts of μ_eff predicted by the extended Maxwell–Garnett theory and (**b**) the frequency band structure normal to the (001) surface of an fcc crystal of $LiTaO_3$ spheres ($S = 2.8\,\mu$m, $\omega_\text{T} = 26.7 \times 10^{12}$ rad/s, $\omega_\text{L} = 46.9 \times 10^{12}$ rad/s, $\varepsilon_\infty = 13.4$) in air as calculated by the rigorous LMS method. The lattice constant is $a = 7.94\,\mu$m. The *solid curve* in (**b**) refers to a degenerate band while the *dotted curve* represents a nondegenerate band

crystal is viewed as a succession of planes parallel to the (001) surface of fcc. Such structures are best modelled by the LMS method, which is an efficient computational method for the study of the EM response of 3D photonic structures consisting of spheres [22, 23] and axisymmetric nonspherical particles [24].

The LMS method is ideally suited for the calculation of the transmission, reflection, and absorption coefficients of an EM wave incident on a composite slab consisting of a number of layers that can be either planes of nonoverlapping particles with the same 2D periodicity or homogeneous plates. For each plane of particles, the method calculates the full multipole expansion of the total multiply scattered wave field and deduces the corresponding transmission and reflection matrices in the plane-wave basis. The transmission and reflection matrices of the composite slab are evaluated from those of the constituent layers. By imposing periodic boundary conditions one can also obtain the (complex) frequency band structure of an infinite periodic crystal. The method applies equally well to nonabsorbing systems and to absorbing ones. Its chief advantage over the other existing numerical methods lies in its efficient and reliable treatment of systems containing strongly dispersive materials such as Drude-like and polaritonic materials.

The crystal is viewed as a stack of two-dimensional crystal layers (planes of spheres) parallel to the (001) surface (which we assume parallel to the xy plane) of an fcc lattice. Note in passing that each crystal layer is a two-dimensional square lattice with the lattice constant $a_0 = a/\sqrt{2}$. For any given $\boldsymbol{k}_\parallel = (k_x, k_y)$, one can calculate the real frequency lines: $k_z = k_z(\omega, \boldsymbol{k}_\parallel)$. Figure 1b shows the frequency band structure, for $\boldsymbol{k}_\parallel = \boldsymbol{0}$ (normal to the (001) surface), for the above-mentioned polaritonic crystal. From Fig. 1b, it is obvious that the LMS frequency band structure predicts a wide photonic band gap from $\omega/\omega_\text{T} = 0.907$ to $\omega/\omega_\text{T} = 0.934$. From $\omega/\omega_\text{T} = 0.934$ to $\omega/\omega_\text{T} = 0.949$ there exists a nondegenerate band and as such, transmission of normally incident light is negligibly small over the frequency region of this band (opti-

cally inactive band) [22]. Within the region of the gap and of the optically inactive bands, one expects to observe a significantly attenuated transmission of light through finite slabs of the above crystal [9]. Therefore one may assume that there exists an effective band gap extending in both regions, i.e., from $\omega/\omega_T = 0.907$ to $\omega/\omega_T = 0.949$. This effective gap almost coincides with the frequency region over which μ_{eff} is negative, i.e., from $\omega/\omega_T = 0.900$ to $\omega/\omega_T = 0.948$. The latter certifies the accuracy of the EMG theory.

The magnetic response demonstrated in Fig. 1 takes place around the transverse phonon frequency ω_T, which lies within the near-infrared regime. Since all ionic materials similar to $LiTaO_3$, e.g., SiC, TlBr, TlCl, exhibit phonon-polariton excitations within this spectral regime (near infrared), if magnetic response in higher frequencies is needed, one has to choose a different class of polariton materials. Such a class of materials are the semiconductors exhibiting exciton-polariton excitations in visible frequencies and even below [13]. For example, Cu_2O possesses a 2P exciton line at 576.84 nm and CuCl possesses a Z_3 exciton line at 386.93 nm [25]. Around the exciton frequencies, the dielectric function of the above semiconductors is given by

$$\varepsilon_s(\omega) = \varepsilon_\infty + A\frac{\gamma}{\omega_0 - \omega - i\gamma}. \qquad (5)$$

The constant A of the (5) is proportional to the exciton oscillation strength; for Cu_2O, $A = 0.02$ while for CuCl, $A = 632$. Since the exciton oscillation strength of the cuprite is rather weak, I will focus on the copper chloride. The rest of the parameters for CuCl, which enter (5) are [25]: $\varepsilon_\infty = 5.59$, $\hbar\omega_0 = 3.363$ eV, and $\hbar\gamma = 5 \times 10^{-5}$ eV. The small value of the loss factor γ implies a very narrow exciton linewidth.

A 3D array consisting of CuCl spheres in air is considered. The radius of the spheres assumes the values $S =$ 10, 20, and 30 nm. The volume filling fraction occupied by the spheres $f = 0.74$ (close-packed arrangement). Arrays of CuCl nanoparticles can be fabricated by colloidal crystallization [26] and ion implantation techniques [27]. Figure 2a and b show the effective magnetic permeability μ_{eff} of the above collection of CuCl spheres, as calculated by (2) and (3), for the above sphere radii. The volume filling fraction has been kept constant, i.e., $f = 0.74$ (close-packed structure), since it ensures the strongest magnetic response for a given sphere radius. The magnetic activity in the region of the exciton resonance stems from the enhancement of the displacement current inside each sphere which, in turn, gives rise to a macroscopic magnetization of the collection of CuCl spheres.

Along with μ_{eff}, Fig. 2c shows the corresponding transmittance curves for slabs of fcc crystals of CuCl spheres for the three different sphere radii. It is clear that, within the frequency regions where μ_{eff} is negative, the corresponding transmittance given by the rigorous LMS method is greatly suppressed, a fact which, again, verifies the validity of the EMG theory. From Fig. 2, it is also evident that as the radius of the CuCl nanoparticles increases, the magnetic resonance becomes more prominent. This is due to the fact that as the radius of the spheres increases, the sphere size parameter x increases accordingly, giving rise to a stronger resonance of T_1^H, and subsequently of μ_{eff}. One also observes that the magnetic resonance (and the transmittance curves accordingly)

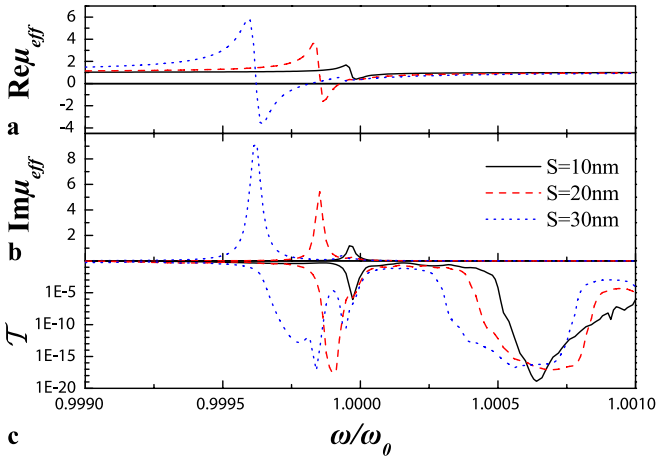

FIGURE 2 Real (**a**) and imaginary (**b**) part of the effective relative permeability μ_{eff} of a collection of close-packed CuCl nanospheres in air, for different radii: $S = 10$ nm (*solid black line*), 20 nm (*red dashed line*) and 30 nm (*blue dotted line*). **c** Transmittance curves for light incident normally on a slab of 16 (001) fcc planes of the above CuCl nanospheres, as calculated by the rigorous LMS method

shift to lower frequencies as the radius increases. This is an expected result, since the poles ω_s of T_1^H (3) move away from ω_0 according to: $\Delta\omega/\omega_0 \sim -(S/c)^2$, where $\Delta\omega = \omega_s - \omega_0$. It is evident that the composite material exhibits magnetic activity around the exciton resonance ω_0, which corresponds to a wavelength of 386.93 nm, approximately 19 times larger than the sphere radius of 20 nm. Since the real part of μ_{eff} assumes negative values, the structure under study is a true subwavelength magnetic metamaterial. Similar but less dramatic effects are expected for arrays of Cu_2O particles.

To conclude this section, it has been shown that in order to obtain magnetic activity in the near-infrared and visible regimes, it is not necessary to resort to sophisticated lithographic techniques [4, 5], since self-assembled arrays of spheres can deliver the desirable property of negative μ_{eff}. Of course, in order to obtain a metamaterial with NRI one has to combine the polaritonic spheres studied above with spheres exhibiting negative ε_{eff} within a common frequency region.

3 Negative refractive index in binary composites

Let us consider the array of $LiTaO_3$ of Fig. 1, which exhibits negative μ_{eff} from $\omega/\omega_T = 0.900$ to $\omega/\omega_T = 0.948$. As stated in the previous section, in order to have an NRI, what is required is a collection of spheres with negative ε_{eff} within all or part of the above negative-μ_{eff} region.

Such spheres would be semiconductor microspheres whose EM response can be modelled in the infrared regime by a Drude-type electric permittivity

$$\varepsilon(\omega) = \varepsilon_0\left(1 - \frac{\omega_p^2}{\omega^2 + i\omega\gamma_2}\right), \qquad (6)$$

where ω_p is the bulk plasma frequency of the semiconductor, γ_2 is the loss factor, and ε_0 is the static dielectric constant. The bulk plasma frequency ω_p is proportional to the square root of the impurity density of the semiconductor [28], which provides the desirable tunability of the EM response

of the spheres. A collection of plasma-type microspheres described by (6) exhibits negative $\varepsilon_{\rm eff}$ in a region around the dipole surface-plasmon frequency $\omega_{\rm sp} = \omega_{\rm p}/\sqrt{1+2/\varepsilon_0}$. As a semiconductor, the choice is n-type Ge with $\varepsilon_0 = 15.8$. Since it is required that the first negative-$\mu_{\rm eff}$ region of the $LiTaO_3$ spheres (see above) coincides with the negative-$\varepsilon_{\rm eff}$ region of the Ge spheres, $\omega_{\rm p}$ is chosen to be the same as $\omega_{\rm T}$. For n-type Ge, this value of $\omega_{\rm p}$ corresponds to an impurity density $N = 3.39\times10^{17}\,{\rm cm}^{-3}$. The radius of the spheres is $S = 2.25\,\mu$m and the volume filling fraction is $f = 0.38$. If the spheres were occupying the sites of an fcc lattice, the corresponding lattice constant would be the same as that derived previously for the polaritonic spheres, i.e., $a = 7.94\,\mu$m. As it was shown recently [9], from $\omega/\omega_{\rm T} = 0.894$ to 0.977, $\varepsilon_{\rm eff}$ of the collection of the n-type Ge becomes negative. This frequency region covers all the negative-$\mu_{\rm eff}$ region of the polaritonic spheres, and therefore, we expect that an NRI will occur in a structure than combines both types of spheres.

In order to see whether a collection of both types of spheres results in an NRI, one must employ an effective medium theory for systems with more than one constituent scatterers. The effective medium parameters of a composite comprising different spheres embedded in a matrix can be obtained from the condition that the average extinction of random unit cells compared with that of the surrounding medium is zero, i.e., the average forward scattering amplitude is zero, $\bar{S}(0) = 0$ [29]. For a composite comprising two different kinds of spheres embedded in a matrix (binary composite) the effective permittivity, $\varepsilon_{\rm eff}$, is given by

$$\sum_{j=A,B} C_j \frac{\varepsilon_{\rm h} - \varepsilon_{\rm eff} - \frac{3i}{2x^3} T^E_{1,j} f_{AB}(2\varepsilon_{\rm h} + \varepsilon_{\rm eff})}{\varepsilon_{\rm h} + 2\varepsilon_{\rm eff} - \frac{3i}{x^3} T^E_{1,j} f_{AB}(\varepsilon_{\rm h} - \varepsilon_{\rm eff})} = 0\,, \tag{7}$$

and the permeability, $\mu_{\rm eff}$ by

$$\sum_{j=A,B} C_j \frac{\mu_{\rm h} - \mu_{\rm eff} - \frac{3i}{2x^3} T^H_{1,j} f_{AB}(2\mu_{\rm h} + \mu_{\rm eff})}{\mu_{\rm h} + 2\mu_{\rm eff} - \frac{3i}{x^3} T^H_{1,j} f_{AB}(\mu_{\rm h} - \mu_{\rm eff})} = 0\,, \tag{8}$$

where f_{AB} is the total filling factor of the spheres and the respective C_A and $C_B = 1 - C_A$ are the concentrations for the spheres A and B. In deriving (7) and (8) it has been assumed that the respective random unit-cell volumes of spheres A and B are proportional to the A and B sphere radii. Equations (7) and (8) are an extension of (8) of [29] to the quasi-static limit and provide a generalization of the earlier expressions for the effective permittivity and permeability, (1) and (2), to the two-sphere composite [9].

Equations (7) and (8) yield a quadratic equation for $\varepsilon_{\rm eff}$ and $\mu_{\rm eff}$, respectively, which can be easily solved. The resulting refractive index $n_{\rm eff} = \sqrt{\varepsilon_{\rm eff}\mu_{\rm eff}}$ for $C_A = C_B = 1/2$ is plotted in Fig. 3a. The complex index of refraction is given by the branch of the square root that yields a nonnegative imaginary part of $n_{\rm eff}$ along the positive real frequency axis. Note in passing that $\varepsilon_{\rm eff}$ and $\mu_{\rm eff}$ are not necessarily both negative within the negative refractive index region due to the imaginary part of $\varepsilon_{\rm eff}$ and $\mu_{\rm eff}$. The refractive index assumes values from $n = -4.81$ at $\omega/\omega_{\rm T} = 0.9038$ to $n = 0$ at $\omega/\omega_{\rm T} = 0.92$. $n = -1$ at $\omega/\omega_{\rm T} = 0.906$.

In order to confirm the occurrence of NRI by using the LMS method, the following periodic structure is considered:

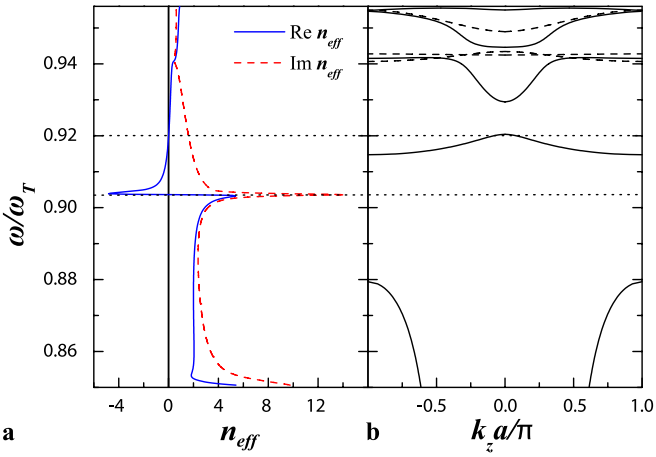

FIGURE 3 (**a**) Real [*solid blue curve*] and imaginary [*dashed red curve*] parts of $n_{\rm eff} = \sqrt{\varepsilon_{\rm eff}\mu_{\rm eff}}$ as given by (7) and (8) for a binary collection of $LiTaO_3$ ($S = 2.8\,\mu$m, $\omega_{\rm T} = 26.7\times10^{12}$ rad/s, $\omega_{\rm L} = 46.9\times10^{12}$ rad/s, $\varepsilon_\infty = 13.4$) and n-type Ge ($S = 2.25\,\mu$m, $\omega_{\rm p} = 26.7\times10^{12}$ rad/s, $\varepsilon_0 = 15.8$) spheres in air. Both type of spheres have the same concentration, i.e., $C_A = C_B = 1/2$ in (7) and (8). The total volume filling fraction f_{AB} occupied by all spheres is $f_{AB} = 0.56$. (**b**) Frequency band structure normal to the fcc (001) surface of an infinite multilayered crystal consisting of alternating planes of $LiTaO_3$ and n-type Ge spheres. The *solid (broken) lines* correspond to degenerate (nondegenerate) frequency bands. The *horizontal dotted lines* define the region where $n_{\rm eff}$ possesses negative real part

a multilayered system that consists of alternating planes of polaritonic and plasmonic spheres [9]. The spheres on each plane occupy the sites of a square lattice and the planes are arranged so that a succession of (001) fcc planes is formed; if the spheres were the same, the resulting structure would become a "monatomic" fcc crystal. Figure 3b shows the frequency band structure for $\boldsymbol{k}_\parallel = \boldsymbol{0}$ [normal to the (001) surface] of the infinite multilayered crystal described above. Again, similarly to Fig. 1b, the solid lines correspond to degenerate (optically active) frequency bands while the broken lines to nondegenerate (optically inactive) ones. One identifies a frequency band extending from $\omega/\omega_{\rm T} = 0.915$ to $\omega/\omega_{\rm T} = 0.92$ where the group velocity $v_{\rm g} = \partial\omega/\partial k_z$ has the opposite sign to the phase velocity $v_{\rm p} = \omega/k_z$; this corresponds to NRI. This NRI frequency band is degenerate and therefore couples with a normally incident EM plane wave. Although the NRI band of Fig. 3b lies almost completely within the NRI region of Fig. 3a, its bandwidth is considerably smaller than the corresponding effective-medium one. The refractive index, $n = {\rm sign}(v_{\rm g})ck_z/\omega$, which corresponds to the NRI band varies monotonically from $n = -2.43$ at the low-frequency edge of the band to $n = 0$ at the higher edge and assumes the value $n = -1$ at $\omega/\omega_{\rm T} = 0.9167$. Again, it is evident that the EMG theory correctly predicts an NRI for the multilayered crystal, although it gives a much wider bandwidth compared to the case of crystals with only polaritonic constituents. It is worth noting that, if one considers a random binary composite instead of the periodic one considered here, an NRI is again present [30].

4 Negative refractive index in metamaterials with chiral symmetry

Next I consider the case of metamaterials exhibiting NRI as a result of their chiral symmetry: when a collec-

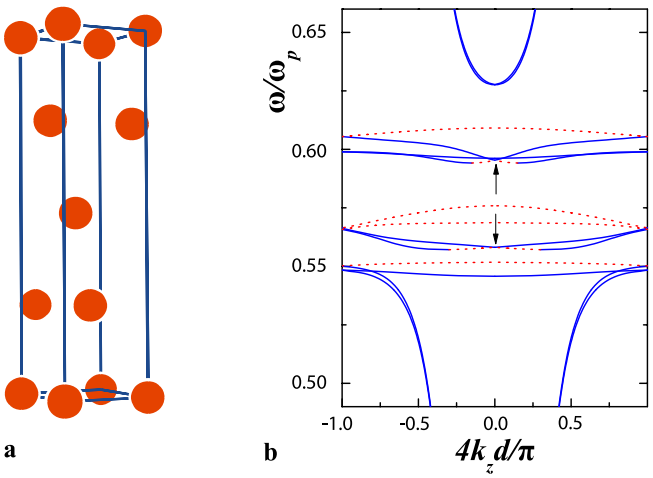

FIGURE 4 (**a**) Unit cell of a tetragonal crystal consisting of four nonprimitive planes of spheres parallel to the (001) surface at positions $(0, 0, 0)$, $(b, 0, d/4)$, $(b, b, d/2)$, and $(0, b, 3d/4)$, with $b = 0.3a$ and $d = 2a$. (**b**) Frequency band structure normal to the (001) surface of the chiral crystal of (**a**). The *broken red lines* correspond to NRI bands and the *solid blue lines* correspond to bands of positive refractive index. The *bands* pointed by the *arrows* are chirality-induced bands

tion of resonant scatterers, e.g., of Drude or Lorentz type, is embedded in a chiral medium then an NRI photon band occurs for one of the polarization modes. More specifically, if such scatterers are placed inside a nonchiral medium a hybridization-induced band gap opens up [31]. Above this gap and at the center of the Brillouin zone, the photon states are triply degenerate (assuming cubic symmetry) as a doubly degenerate (of transverse nature) and a nondegenerate (of longitudinal nature) photon band coincide. When the medium hosting the scatterers is chiral, the doubly degenerate (transverse) band above the gap splits into two nondegenerate bands creating the NRI part of the dispersion relation [15, 16].

A crystal of Drude-type spheres in helical configuration is considered. The unit cell of the crystal is shown in Fig. 4a and can be described as a tetragonal crystal with a four-point basis. The crystal is viewed as a succession of planes of spheres parallel to the xy-plane. Each plane possesses the same 2D periodicity defined by the primitive vectors $\boldsymbol{a}_1 = (a, 0, 0)$ and $\boldsymbol{a}_2 = (0, a, 0)$ [(001) crystallographic surface]. A unit layer of the crystal consists of four nonprimitive planes of spheres at $(0, 0, 0)$, $(b, 0, d/4)$, $(b, b, d/2)$, and $(0, b, 3d/4)$. The $(n+1)$-th unit layer is obtained from the n-th layer by the primitive translation $\boldsymbol{a}_3 = (0, 0, d)$. Such a structure (one with dielectric spheres) was originally suggested by Karathanos et al. [32] as an artificial chiral material that can be used for rotating the plane of polarization of linearly polarized light.

The spheres of the crystal of Fig. 4a are of radius $S = 0.2a$ and their dielectric function is of Drude metallic type, i.e., it is given by (6) with $\varepsilon_0 = 1$. The lattice constant a of the 2D square lattice is taken to be $a = c/\omega_\mathrm{p}$. For example, for gold $\hbar\omega_\mathrm{p} = 8.99$ eV corresponding to a lattice constant $a = 22$ nm and sphere radius $S = 4.4$ nm. Losses are turned off by setting $\gamma_2 = 0$ in (6). Note that, this particular choice of dielectric function is not essential for the occurrence of NRI; other types of dielectric function such as those of (4) or (5) are expected to result in an NRI.

In order to discover NRI frequency regions for the crystal of Fig. 4a, a frequency band structure calculation is needed using the LMS method. Figure 4b shows the frequency band structure, for $\boldsymbol{k}_\parallel = \boldsymbol{0}$ (normal to the (001) surface), of the crystal with unit cell that of Fig. 4a with $b = 0.3a$ and $d = 2a$. All bands appearing in Fig. 4a are nondegenerate due to the chiral symmetry of the crystal. One identifies six frequency bands corresponding to NRI. The first NRI band extends from $\omega/\omega_\mathrm{p} = 0.55$–$0.552$, the second from 0.557 to 0.558, the third from 0.566–0.568, the fourth from 0.566–0.576, the fifth from 0.594 to 0.595 and the sixth from 0.605–0.609. As expected, the NRI frequency bands are developed around the surface plasma modes of a single Drude nanosphere; as a result, the NRI bands lie in the optical regime since the surface plasma frequency $\omega_{sp} = \omega_\mathrm{p}/\sqrt{3}$ of noble metal nanoparticles lies in this frequency region. The second and the fifth band (also pointed by the arrows) are chirality-induced bands since they disappear when chirality is lost by setting $b = 0.5a$ instead of $b = 0.3a$ in the unit cell of the crystal of Fig. 4a [15]. These chirality-induced bands result from the splitting of the triple degeneracy of the photonic bands at the Brillouin zone center (see above).

5 Conclusions

Using both effective medium theory and rigorous computational methods it has been shown that collections of phonon-polaritonic spheres and exciton-polaritonic spheres exhibit strong magnetic response in the near-infrared and near-optical regimes, respectively. When polaritonic spheres are mixed with plasmonic spheres, in order to form a binary composite, an NRI can result. An NRI can also be generated when plasmonic or polaritonic spheres alone are arranged in space so as to form a crystal of chiral symmetry. In this case, multiple NRI bands arise around the characteristic resonance of the spheres.

ACKNOWLEDGEMENTS This work has been supported by the European Union's Transfer of Knowledge project CAMEL (Grant No. MTKD-CT-2004-014427).

REFERENCES

1 V.G. Veselago, Sov. Phys. Uspekhi **10**, 509 (1968)
2 J.B. Pendry, Phys. Rev. Lett. **85**, 3966 (2000)
3 J.B. Pendry, Contemp. Phys. **45**, 191 (2004)
4 T.J. Yen, W.J. Padilla, N. Fang, D.C. Vier, D.R. Smith, J.B. Pendry, D.N. Basov, Science **303**, 1494 (2004)
5 S. Linden, C. Enkrich, M. Wegener, J. Zhou, T. Koschny, C.M. Soukoulis, Science **306**, 1351 (2004)
6 R.A. Shelby, D.R. Smith, S. Schultz, Science **292**, 77 (2001)
7 C.G. Parazzoli, R.B. Greegor, K. Li, B.E.C. Koltenbah, M. Tanielian, Phys. Rev. Lett. **90**, 107 401 (2003)
8 A.A. Houck, J.B. Brock, I.L. Chuang, Phys. Rev. Lett. **90**, 137 401 (2003)
9 V. Yannopapas, A. Moroz, J. Phys.: Condens. Matter **17**, 3717 (2005)
10 M.S. Wheeler, J.S. Aitchison, M. Mojahedi, Phys. Rev. B **72**, 193 103 (2005)
11 M.S. Wheeler, J.S. Aitchison, M. Mojahedi, Phys. Rev. B **73**, 045 105 (2005)
12 L. Jylhä, I. Kolmakov, S. Maslovski, S. Tretyakov, J. Appl. Phys. **99**, 043 102 (2006)
13 V. Yannopapas, N.V. Vitanov, Phys. Rev. B **74**, 193 304 (2006)
14 T.G. Mackay, A. Lakhtakia, J. Appl. Phys. **100**, 063 533 (2006)
15 V. Yannopapas, J. Phys.: Condens. Matter **18**, 6883 (2006)
16 J.B. Pendry, Science **306**, 1353 (2004)

17 S. Tretyakov, A. Shivola, L. Jylhä, Photon. Nanostruct. **3**, 107 (2005)
18 W.T. Doyle, Phys. Rev. B **39**, 9852 (1989)
19 R. Ruppin, Opt. Commun. **182**, 273 (2000)
20 H. Ibach, H. Lüth, *Solid-State Physics* (Springer, Berlin, 2003)
21 M. Schall, H. Helm, S.R. Keiding, Int. J. Infrared Milli. **20**, 595 (1999)
22 N. Stefanou, V. Karathanos, A. Modinos, J. Phys.: Condens. Matter **4**, 7389 (1992)
23 N. Stefanou, V. Yannopapas, A. Modinos, Comput. Phys. Commun. **113**, 49 (1998); **132**, 189 (2000)
24 G. Gantzounis, N. Stefanou, Phys. Rev. B **73**, 035 115 (2006)
25 M. Artoni, G. La Rocca, F. Bassani, Phys. Rev. E **72**, 046 604 (2005)
26 Z.C. Orel, E. Matijević, D.V. Goia, Colloid Polym. Sci. **281**, 754 (2003)
27 K. Fukumi, A. Chayahara, H. Kageyama, K. Kadono, T. Akai, N. Kitamura, H. Mizoguchi, Y. Horino, M. Makihara, K. Fujii, J. Hayakawa, J. Non-Cryst. Solids **259**, 93 (1999)
28 D.K. Schroeder, *Semiconductor Material and Device Characterization* (Wiley, New York, 1990)
29 R. Luo, Appl. Opt. **36**, 8153 (1997)
30 V. Yannopapas, Phys. Rev. B **75**, 035112 (2007)
31 V. Yannopapas, A. Modinos, N. Stefanou, Phys. Rev. B **60**, 5359 (1999)
32 V. Karathanos, N. Stefanou, A. Modinos, J. Mod. Opt. **42**, 619 (1995)